

Microbeam high angular resolution x-ray diffraction in InGaN/GaN selective-area-grown ridge structures

A. A. Sirenko^{a)}

Department of Physics, New Jersey Institute of Technology, Newark, New Jersey 07102

A. Kazimirov, S. Cornaby, and D. H. Bilderback

Cornell High Energy Synchrotron Source (CHESS), Cornell University, Ithaca, New York 14853

B. Neubert, P. Brückner, and F. Scholz

Optoelectronics Department, University of Ulm, 89081 Ulm, Germany

V. Shneidman

Department of Physics, New Jersey Institute of Technology, Newark, New Jersey 07102

A. Ougazzaden

Georgia Institute of Technology/GTL, UMI 2958 Georgia Tech-CNRS, 57070 Metz, France

(Received 6 August 2006; accepted 20 September 2006; published online 3 November 2006)

GaN-based 6- μm -wide ridge waveguides with InGaN/GaN multiple-quantum-wells (MQWs) produced by metal organic vapor-phase epitaxy in the regime of selective-area growth have been studied with microbeam high angular resolution x-ray diffraction and reciprocal-space mapping. Variation of the strain from 0.9% to 1.05% and a factor of 3 for the thickness enhancement of the MQW period have been measured for different widths of the oxide mask surrounding the GaN-based ridges. Only when the trapezoidal shape of the ridge cross section is taken into account can the difference between the experimentally measured thickness enhancement and predictions of the long-range gas-phase diffusion model be reconciled. © 2006 American Institute of Physics. [DOI: 10.1063/1.2378558]

Selective-area growth¹⁻⁴ (SAG) is a powerful technique for monolithic integration of multifunctional structures with complementary optical and electronic properties. The structural quality and optical efficiency of GaN-based materials can be improved using the SAG technique taking advantage of the strain relaxation and reduced piezoelectric field at the sidewalls of selectively grown ridges.⁵⁻⁷ Adequate characterization tools, such as synchrotron radiation based microbeam high-resolution x-ray diffraction (HRXRD),⁸⁻¹¹ are required for detailed analysis of the fundamental growth mechanisms of GaN-based SAG structures. In this letter we apply nondestructive HRXRD technique and reciprocal-space-mapping (RSM) analysis with a spatial resolution on a micron scale to determine the thickness, strain, and composition variation in various SAG ridge structures with InGaN/GaN multiple-quantum-wells (MQWs).

Samples were grown on a *c*-plane sapphire substrate using low-pressure metal organic vapor-phase epitaxy in a single-wafer Aixtron system.⁷ Planar growth of a (0001) oriented GaN template layer was followed by deposition of SiO₂ mask arrays. The width of the oxide mask stripes *A* varied between 2 and 20 μm for different arrays of 20 identical oxide stripes separated by the same opening *B* of 6 μm and oriented along the $\langle 11\bar{2}0 \rangle$ direction. The second growth step was a selective epitaxy process inside the 6- μm -wide open parts of the wafer producing trapezoidal ridges with the (0001) orientation of the top plane and $\{1\bar{1}01\}$ orientation of the sidewalls. SAG ridges consisted of a few micron thick *n*-GaN layer grown at 1020 °C followed by the active region grown at 800 °C and a thin GaN:Mg top layer grown again

at 1020 °C. The multiple-quantum-well active region had five InGaN quantum wells ($N=5$) separated by GaN barriers.

HRXRD characterization was carried out at the A2 beamline at CHESS (Fig. 1) equipped with a one-bounce focusing capillary BSG7 with the x-ray beam size of 10 μm , tip-to-focus working distance of 30 mm, and divergence of 800 arc sec.¹² The diffraction measurements were performed at an energy of 12.4 keV. SAG ridges were oriented along the diffraction plane so that in each measurement we collected diffracted signal from a single ridge.¹³ High angular resolution was provided by a combination of a perfect Ge(111) crystal analyzer and a two-bounce Ge(111) channel cut crystal with the full width at half maximum (FWHM) of the “intrinsic” rocking curve of 13 arc sec. The channel cut crystal was positioned between the capillary and the sample to condition the incident beam for the high-resolution RSM analysis.¹¹ By performing θ - 2θ scans, where θ and 2θ denote rotation angles of the sample and the detector arm, respectively, the diffraction profiles were measured around 0002 reflection of GaN with $\theta_{\text{Bragg}}=11.12$ deg over a wide range of $\Delta\theta \approx 1$ deg.

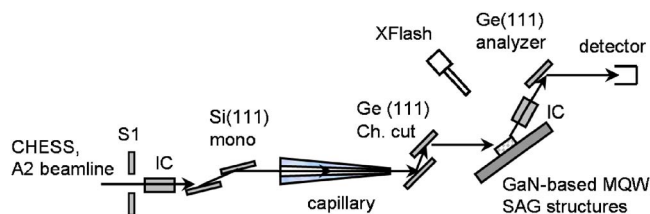


FIG. 1. (Color online) HRXRD setup at the CHESS A2 beamline consists of the upstream slit S1, ion chambers IC, Si(111) monochromator, XFlash fluorescence detector, one-bounce focusing capillary, single-bounce Ge(111) analyzer, and Ge(111) channel cut crystals.

^{a)}Electronic mail: sirenko@njit.edu

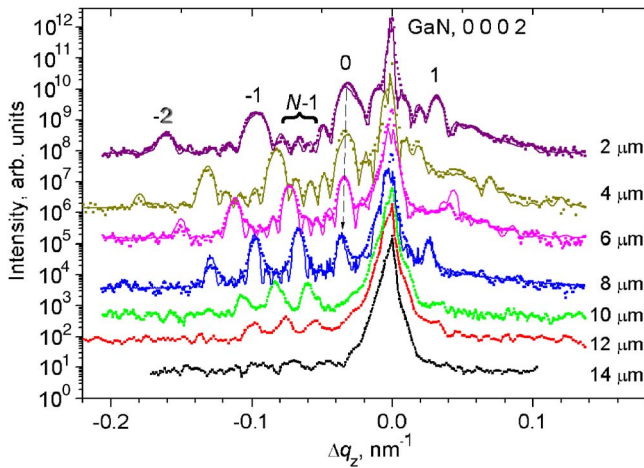


FIG. 2. (Color online) (a) X-ray diffraction (solid squares) from the InGaN/GaN MQW 6-μm-wide SAG ridges for arrays with different widths of the oxide mask A marked next to the curves (2 μm, 4 μm, ...). The diffraction curves are vertically offset for clarity. The substrate GaN 0002 peak is at θ_{Bragg}=11.12 deg. The arrow shows the shift of the zeroth-order MQW global-strain peak. Simulated HRXRD spectra for the SAG structures with A=2, 4, 6, and 8 μm are shown with solid curves.

Figure 2 shows diffraction profiles measured in the center of the SAG ridges for the ridges with different width, of the oxide mask: A=2, 4, 6, ..., 14 μm. The separation of the superlattice peaks (e.g., between “-2” and “-1” peaks) determines the MQW period P=W_W+W_B, while the relative position of the MQW zeroth-order peak with respect to the GaN 0002 layer peak corresponds to the global strain of the MQW structure: S=W_WS_W/(W_W+W_B), where W_{W(B)} and S_W are the thickness and strain of the well (barrier), respectively. The (N-1) Kiessig fringes between the superlattice “-1” and “0” peaks indicate a high angular resolution of our setup and an efficient suppression of the diffused background. Similar to the procedure applied before to InP-based SAG structures,¹⁰ we determined the thickness of the individual well and barrier layers using RADS-MERCURY BEDE software based on the dynamic diffraction theory for x-ray diffraction.¹⁴ No MQW-related XRD signal was detected for the structures with the width of the oxide mask A more than 14 μm. Our scanning electron microscopy (SEM) results show that the ridges grown with this periodicity are not trapezoidal, but purely triangular without a flat MQW region at the top.⁷

The main parameters of investigated SAG MQWs are shown in Fig. 3. An increase of the oxide mask width from 2 to 12 μm resulted in the changes of the MQW period P from 16 to 46 nm [Fig. 3(a)]. Correspondingly, the width of the well and barrier layers increases, as shown in Fig. 3(b). The thickness enhancement for InGaN quantum wells W_W(A) × [nm]=3.8(1+0.3A[μm]) is very close to that for the GaN barrier W_B(A)[nm]=5.6(1+0.3A[μm]), where the interpolated values of the well and barrier thickness for the unmasked growth (A=0) are 3.8 and 5.6 nm, respectively, and 0.3 nm/μm is the slope determined with the error bar of ±0.03 nm/μm.

As it is known for selective growth of III-V arsenide- and phosphide-based compounds (e.g., InGaAsP), the vertical and lateral vapor-phase diffusion processes (VVP and LVP, respectively) and the surface migration of the metal organic precursors are the three main mechanisms with dif-

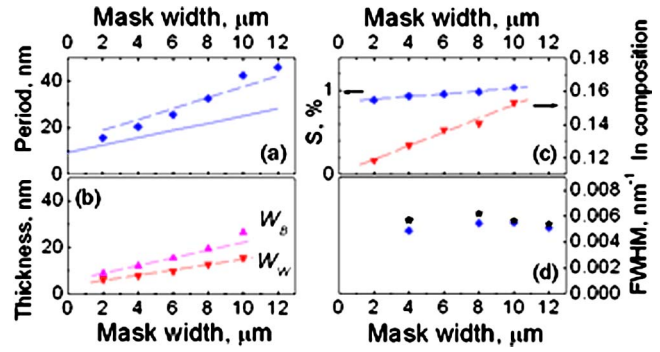


FIG. 3. (Color online) (a) Period of the MQWs vs A (diamonds). The solid and dashed straight lines represent different models for the growth enhancement (see text for details). (b) The thickness of the quantum wells W_W (down triangles) and barriers W_B (up triangles). The dashed straight lines represent linear fits to the experimental data. (c) Left scale: Composite strain S of the 6-μm-wide MQW SAG structures. Right scale: The indium composition in the InGaN quantum wells. (d) FWHM for the MQW (diamonds) and GaN peaks (stars) measured along the q_y direction in the RSMs (see Fig. 5).

ferent characteristic lengths that result in the thickness enhancement and compositional changes in the SAG regime.^{2,3,9,15,16} The gas-phase diffusion model allows accurate calculations of the VVP and LVP effects with characteristic diffusion lengths D_v/k in the range of 20–200 μm, while the surface migration effect is important for the analysis of the ridge shape and composition on the scale of a few microns.^{9,15} Analysis of the thickness enhancement for the experimentally measured MQW period P [Fig. 3(a)] is simplified in our case by the periodic array geometry of the oxide mask. Indeed, the gas-phase diffusion model, which otherwise requires the knowledge of the diffusion lengths D_v/k for the group-III precursors (In, Ga), has a simple analytical solution for periodic arrays. In this case, the growth enhancement P/P₀ is limited by the mask load and for the SAG process with D_v/k(In, Ga) ≫ A+B it cannot exceed (A+B)/B, where P₀ corresponds to the unmasked growth. However, the corresponding dependence [solid line in Fig. 3(a)] demonstrates a significant discrepancy with our experimental points. We attempted to compensate for this difference by introducing a correction factor taking into account the real trapezoidal shape of the ridge cross section—a complication that is usually ignored in the gas-phase diffusion model. As one can see in Fig. 4, the actual width of the MQW section that is located at the top of the ridge (marked with b) is less than the nominal distance between the oxide mask stripes B. Correspondingly, the growth enhancement should be changed to (A+B)/b.¹⁷ Indeed, the straight dashed

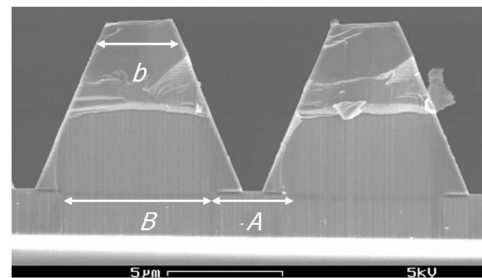


FIG. 4. SEM photograph of the SAG ridges with A=4 μm and B=6 μm. The MQW section of the structure with five InGaN wells is not well resolved on the top facet due to a low (~0.12) fraction of indium.

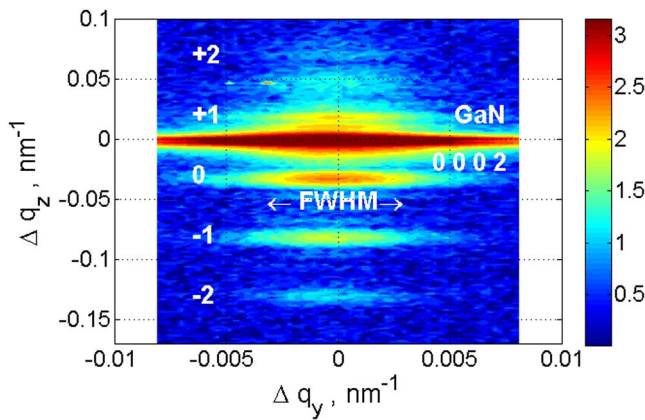


FIG. 5. (Color online) Reciprocal-space map for 0 0 2 reflection with the GaN substrate peak and MQW satellite peaks marked according to their order. The horizontal arrow shows the FWHM of the satellite MQW peak.

line in Fig. 3(a), which is calculated for $b=4\ \mu\text{m}$, shows a better agreement with experiment. Thus, our results demonstrate that the long-range gas-phase diffusion model alone cannot provide a reliable quantitative description of experiment for the micron-wide ridge formation in the SAG regime for nitrides. Surface migration, which results in a different growth rate on the trapezoidal ridge facets, has to be taken into account.

Figure 3(c) shows that the global strain of the MQW structures changes from 0.9% to 1.05% when A varies from 2 to 12 μm . Here the MQW strain is expressed in terms of the perpendicular d -spacing mismatch ($S=\Delta d/d$) with respect to the GaN substrate. It is natural to attribute this effect to the variation of indium composition in the InGaN quantum wells. The indium composition could be straightforwardly determined from the diffracted profiles (Fig. 2), but first we need to provide an additional proof that the measured strain is elastic, especially for the ridges with the wide oxide mask. Indeed, the quantum well width W_w increases strongly with increasing A and for $A=10\ \mu\text{m}$ the total thickness of InGaN layers NW_w approaches 75 nm, which is close to the critical thickness of $75\pm 7\ \text{nm}$ for $\text{In}_{0.15}\text{Ga}_{0.85}\text{N}$ single layers grown on GaN.¹⁸ However, our earlier photoluminescence studies⁷ and x-ray data show no indication that the quantum wells change from strained to relaxed.

RSM is an ideal tool to study strain and its relaxation in lattice-mismatched heterostructures. Figure 5 shows RSM for the SAG ridge with $A=4\ \mu\text{m}$. The MQW peaks are marked according to their order. The FWHM for the MQW peaks measured along the q_y direction (close to the θ direction in the angular space) is very close to that for the GaN peak. Figure 3(d) shows that similar values of FWHM were observed for all investigated SAG ridges indicating that no additional mosaic spread was introduced during the SAG process compared to the mosaicity of the GaN template substrate. Note that a significant increase of the FWHM values for MQWs in Fig. 3(d) should be expected in the case of developing strain relaxation. We therefore conclude that all our MQWs are pseudomorphically strained as a consequence of the fairly thick GaN barriers between InGaN quantum

wells, which decouple the quantum wells and hence increase the critical thickness of the whole package. Assuming that the measured strain in MQWs is indeed elastic, the indium composition in the InGaN quantum wells changes from 0.12 to 0.15 in the SAG structures with A between 2 and 10 μm [Fig. 3(c)]. The observed increase of indium composition can imply that the gas-phase diffusion coefficient of indium is smaller than that for gallium. Additional contribution to the observed increase of In composition at the top facet could be due to a relatively high rate of In interfacet migration (from $\{1\bar{1}01\}$ -oriented sidewalls to 0001-oriented top facet) compared to that for Ga.¹⁹ In the future, we plan to determine $D_v/k(\text{In,Ga})$ and the interfacet migration rates by performing accurate cross-section HRXRD studies of GaN-based SAG ridges with a submicron size of the x-ray beam.

The Cornell High Energy Synchrotron Source is supported by the National Science Foundation and the National Institutes of Health/National Institute of General Medical Sciences under Award No. DMR-0225180.

- ¹J. J. Coleman, R. M. Lammert, M. L. Osowski, and A. M. Jones, IEEE J. Sel. Top. Quantum Electron. **3**, 874 (1997).
- ²T. Van Caenegem, I. Moerman, and P. Demeester, Prog. Cryst. Growth Charact. Mater. **35**, 263 (1997).
- ³M. Gibbon, J. P. Stagg, C. G. Cureton, E. J. Thrush, C. J. Jones, R. E. Mallard, R. E. Pritchard, N. Collis, and A. Chew, Semicond. Sci. Technol. **8**, 998 (1993).
- ⁴M. A. Alam, R. People, E. D. Isaacs, K. Evans-Lutterodt, T. Siegrist, T. Pernell, J. Vandenberg, S. K. Sputz, S. N. G. Chu, D. V. Lang, L. Smith, and M. Hybertsen, Appl. Phys. Lett. **74**, 2617 (1999).
- ⁵L. S. Wang, S. Tripathy, B. Z. Wang, J. H. Teng, S. Y. Chow, and S. J. Chua, Appl. Phys. Lett. **89**, 011901 (2006).
- ⁶O. Ambacher, J. Phys. D **31**, 2653 (1998).
- ⁷B. Neubert, P. Brückner, F. Habel, F. Scholz, T. Riemann, J. Christen, M. Beer, and J. Zweck, Appl. Phys. Lett. **87**, 182111 (2005).
- ⁸A. Kazimirov, A. A. Sirenko, D. H. Bilderback, Z.-H. Cai, B. Lai, R. Huang, and A. Ougazzaden, J. Phys. D **39**, 1 (2006).
- ⁹A. A. Sirenko, A. Kazimirov, A. Ougazzaden, S. O'Malley, D. H. Bilderback, Z.-H. Cai, B. Lai, R. Huang, V. Gupta, M. Chien, and S. N. G. Chu, Appl. Phys. Lett. **88**, 081111 (2006).
- ¹⁰A. A. Sirenko, A. Kazimirov, R. Huang, D. H. Bilderback, S. O'Malley, V. Gupta, K. Bacher, L. J. P. Ketelsen, and A. Ougazzaden, J. Appl. Phys. **97**, 063512 (2005).
- ¹¹A. Kazimirov, R. Huang, D. Bilderback, A. A. Sirenko, and A. Ougazzaden, J. Phys. D **37**, L1 (2004).
- ¹²D. H. Bilderback and E. Fontes, AIP Conf. Proc. **417**, 147 (1997).
- ¹³Since the x-ray beam of 10 μm is wider than the top part of the trapezoidal ridge, all diffraction curves have an additional contribution from the masked part of the GaN substrate and the sidewalls. However, this contribution does not affect the x-ray data analysis for the top part of the MQWs.
- ¹⁴M. Wormington, C. Panaccione, K. M. Matney, and K. D. Bowen, Philos. Trans. R. Soc. London, Ser. A **357**, 2827 (1999).
- ¹⁵S. Kitamura, K. Hiramatsu, and N. Sawaki, Jpn. J. Appl. Phys., Part 2 **34**, L1184 (1995).
- ¹⁶F. Scholz, D. Ottenwälder, M. Eckel, M. Wild, G. Frankowsky, T. Wacker, and A. Hangleiter, J. Cryst. Growth **145**, 242 (1994).
- ¹⁷As it has been shown in Ref. 7, the MQW growth on the ridge sidewalls is a much slower process and thus its contribution is neglected in this qualitative analysis.
- ¹⁸C. A. Parker, J. C. Roberts, S. M. Bedair, M. J. Reed, S. X. Liu, and N. A. El-Masry, Appl. Phys. Lett. **75**, 2776 (1999).
- ¹⁹M. Funato, T. Kotani, T. Kondou, Y. Kawakami, Y. Narukawa, and T. Mukai, Appl. Phys. Lett. **88**, 261920 (2006).